

# Mechanistic Insights into Fe Catalyzed $\alpha$ -C-H Oxidations of Tertiary Amines

Christopher J. Legacy,<sup>a</sup> Frederick T. Greenaway,<sup>b</sup> Marion H. Emmert<sup>a,c\*</sup>

<sup>a</sup>Department of Chemistry and Biochemistry, Worcester Polytechnic Institute, 100 Institute Road, Worcester, MA 01609, USA

<sup>b</sup>EPR studies. Gustaf H. Carlson School of Chemistry, Clark University, 950 Main Street, Worcester, MA 01610, USA

<sup>c</sup>Current Address: Department of Process Research & Development, Discovery Process Chemistry, MRL, Merck & Co., Inc., 770 Sumneytown Pike, West Point, PA 19486, USA

**ABSTRACT:** We report detailed mechanistic investigations of an iron-based catalyst system, which allows the  $\alpha$ -C-H oxidation of a wide variety of amines, including acyclic tertiary aliphatic amines, to afford dealkylated or amide products. In contrast to other catalysts that affect  $\alpha$ -C-H oxidations of tertiary amines, the system under investigation employs exclusively peroxy esters as oxidants. More common oxidants (e.g. <sup>t</sup>BuOOH) previously reported to affect amine oxidations via free radical pathways do not provide amine  $\alpha$ -C-H oxidation products in combination with the herein described catalyst system. Motivated by this difference in reactivity to more common free radical systems, the investigations described herein employ initial rate kinetics, kinetic profiling, Eyring studies, kinetic isotope effect studies, Hammett studies, ligand coordination studies, and EPR studies to shed light on the Fe catalyst system. The obtained data suggest that the catalytic mechanism proceeds through C-H abstraction at a coordinated substrate molecule. This rate-determining step occurs either at an Fe(IV) oxo pathway or a 2-electron pathway at a Fe(II) intermediate with bound oxidant. We further show via kinetic profiling and EPR studies that catalyst activation follows a radical pathway, which is initiated by hydrolysis of PhCO<sub>3</sub><sup>t</sup>Bu to <sup>t</sup>BuOOH in the reaction mixture. Overall, the obtained mechanistic data support a non-classical, Fe catalyzed pathway that requires substrate binding, thus inducing selectivity for  $\alpha$ -C-H functionalization.

## Introduction

C-H oxidations of organic molecules frequently occur in biosynthetic pathways<sup>1</sup> as well as in drug metabolism.<sup>2</sup> Many of these reactions are catalyzed by enzymes bearing Fe cofactors. Examples are the cytochrome P<sub>450</sub> family exhibiting Fe-porphyrin cofactors<sup>2-4</sup> or non-heme dioxygenases, hydroxylases, and halogenases.<sup>5</sup> The majority of these systems catalyze oxidations via Fe(IV) oxo intermediates, which attack aliphatic C-H bonds of a substrate in a radical rebound fashion, cleaving the C-H bond via a hydrogen abstraction mechanism.<sup>5,2,6-9</sup> For enzyme-catalyzed amine  $\alpha$ -C-H oxidations, an alternative mechanistic possibility to Fe oxo pathways has been proposed, based on model compound studies.<sup>10</sup> This mechanism proceeds through single electron and proton transfers, forming iminium or imine products via radical intermediates.

The mechanistic framework of *synthetic* systems that functionally mimic the metabolic pathways of amine  $\alpha$ -C-H oxidations in combination with O<sub>2</sub>, H<sub>2</sub>O<sub>2</sub>, or <sup>t</sup>BuOOH as oxidants have long been under discussion, with proposed pathways proceeding via free or solvent-caged radicals, hemiaminals, perox-hemiaminals, and/or metal-coordinated iminium ions.<sup>11-18</sup> Recently, a seminal publication by Doyle and coworkers has shown that the majority of the catalysts employing <sup>t</sup>BuOOH as oxidant likely promote oxidations via free radical pathways and hemiaminal intermediates, regardless of the used metal catalyst.<sup>19</sup> This study was performed with aniline-type substrates and the investigated catalysts included both precious metal systems (Rh<sub>2</sub>(cap)<sub>4</sub>, RuCl<sub>3</sub>) and base-metal catalysts (CuBr, FeCl<sub>3</sub>,

Co(OAc)<sub>2</sub>). Importantly, the presence of O<sub>2</sub> influenced the kinetic isotope effects observed, suggesting that reaction pathways may differ depending on the used oxidant. Unfortunately, the question of whether the mechanistic insights reported by Doyle and coworkers are transferrable to  $\alpha$ -C-H functionalizations of *aliphatic* amines has not been resolved yet, as many catalysts active in aniline  $\alpha$ -C-H oxidations are unreactive towards tertiary aliphatic amines.<sup>20</sup>

Motivated by the absence of such mechanistic information regarding the  $\alpha$ -C-H oxidations of aliphatic amines, we set out to establish mechanistic hypotheses supported by experimental data for a Fe-based catalyst system previously developed in our lab (see Scheme 1).



**Scheme 1. Optimized Conditions for Fe Catalyzed  $\alpha$ -C-H oxidation of Tertiary Aliphatic Amines.**

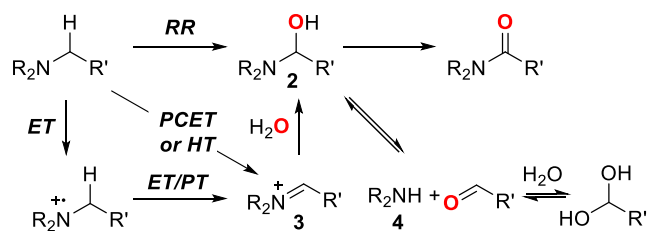
This reaction affects oxidations of aromatic *and* aliphatic amines and is selective for  $\alpha$ -C-H functionalizations of amines, even in complex molecule settings such as active pharmaceutical ingredients.<sup>20</sup> Surprisingly, many common oxidants

previously used in Fe oxidation catalysis do not affect this reaction, with the exception of peroxyesters that afford between 21% and 71% yield. Yields are strongly dependent on the steric bulk of the amine substrate. In contrast to other protocols proceeding via free radical pathways,<sup>21</sup> the established reaction conditions are selective for oxidation of C-H bonds of *acyclic* substrates, while cyclic  $\alpha$ -C-H bonds are not attacked

Based on the studies detailed in this manuscript, we propose that  $\alpha$ -C-H cleavage proceeds through a radical rebound or concerted mechanism instead of a free radical mechanism often proposed with simple Fe catalysts such as in Fenton-type chemistries.<sup>22</sup> Interestingly, the experimental values for Eyring parameters and kinetic isotope effect (KIE) are more akin to values typically observed with  $\beta$ -hydride elimination (formal hydride shift) and concerted metalation deprotonation (involvement of a heteroatom of the oxidant). Such two-electron processes are most often invoked for C-H cleavage processes in precious metal catalysts (e.g. Pd, Ir<sup>23,24</sup>). This mechanistic proposal provides insight into the need for peroxyester oxidants, the role of each reaction component under the empirically established optimal catalytic conditions, and the sources of side products observed in the reaction mixture. Overall, the mechanistic pathway provides a rationale for the selectivity of amine  $\alpha$ -C-H oxidation with the established Fe catalyst system.

## Results and Discussion

**A. General Mechanistic Framework for Fe Catalyzed Amine to Amide Conversion.** Our laboratory has previously<sup>20</sup> reported several key mechanistic features of the Fe catalyzed  $\alpha$ -C-H oxidation of amines (see Scheme 2: (1) The concentration of H<sub>2</sub>O had been found to be crucial for high conversion, with loadings of less than 5 equiv. and more than 15 equiv. significantly reducing amide yields. (2) In reactions with large amounts of H<sub>2</sub>O added, the major side product is dealkylated amine **4**; lowering the oxidant (PhCO<sub>3</sub>tBu) loading leads to formation of up to 64% of **4**. Furthermore, aldehyde side products can be observed. (3) Reactions performed in the presence of H<sub>2</sub><sup>18</sup>O as additive revealed that the oxygen atom incorporated in the amide product stems from H<sub>2</sub>O (and not O<sub>2</sub> or PhCO<sub>3</sub>tBu). (4) Experiments performed in the presence of KCN led to  $\alpha$ -C-H cyanation instead of  $\alpha$ -C-H oxygenation, suggesting that iminium compounds **3** are potential intermediates or side products in the reaction pathway.



**Scheme 2. General Reaction Framework.** RR = radical rebound; PCET = proton-coupled electron transfer; HT = hydride transfer; ET = electron transfer; PT = proton transfer.

(5) Finally, reacting HNPr<sub>2</sub> and EtCHO under analogous reaction conditions to amine  $\alpha$ -C-H oxidation conditions also resulted in formation of the corresponding amide. Collectively, these findings supported the proposal of a mechanistic framework for amine  $\alpha$ -C-H oxidation as formulated in Scheme 2 in

analogy to aniline oxidation pathways affected by Fe-heme compounds.<sup>10</sup>

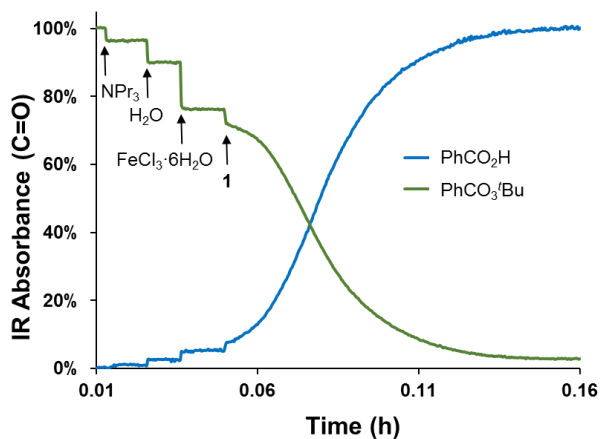
In the proposed mechanistic pathway, the initial C-H bond cleavage may proceed through a radical rebound mechanism (RR, Scheme 2, top), providing direct access to hemiaminal **2**. Alternatively, a proton-coupled electron transfer (PCET) or hydride transfer (HT; Scheme 2, middle) or a sequence of electron and proton transfers (ET/PT, bottom) may form the iminium intermediate **3**, which in turn is attacked by H<sub>2</sub>O to provide hemiaminal **2**. In the presence of large amounts of H<sub>2</sub>O in the reaction solution, dealkylation of amine substrate to afford **4** is likely driven by formation of the aldehyde hydrate; alternatively, a second  $\alpha$ -C-H oxidation of hemiaminal **2** would result in formation of the amide product. These preliminary mechanistic investigations did not provide any insight into the first, most crucial part of amine  $\alpha$ -C-H oxygenation: the process of  $\alpha$ -C-H bond breaking and the role of the catalyst in this process. As such, our subsequent studies aimed to elucidate this question.

**B. Initial Rate Kinetics.** We first sought to establish an experimental kinetic rate law, using the method of initial rates. We reasoned that this approach would provide a suitable framework for further mechanistic studies, eventually leading to rational optimization of the amine  $\alpha$ -C-H oxidation protocol and new catalyst developments. Due to the paramagnetic properties of the Fe catalyst used in amine  $\alpha$ -C-H oxidation, the use of NMR techniques to follow the kinetic profile of the reactions was deemed unsuitable. Instead, *in-situ* FTIR was employed and the disappearing C=O band of the oxidant (PhCO<sub>3</sub>tBu) was observed to provide well-characterized kinetic profiles.

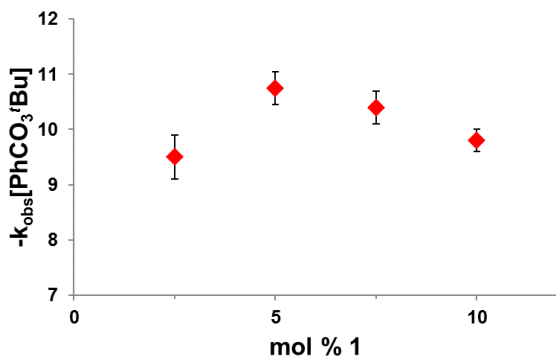
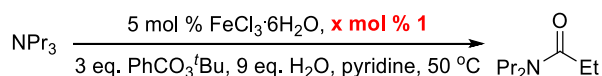
We first explored the role of the added ligand **1** for catalysis. To this end, the oxidant PhCO<sub>3</sub>tBu was added to pyridine as solvent and an *in-situ* FTIR signal was established. This signal (represented by the green line in Scheme 3) showed initially a curve without any slope, signifying the absence of reactivity. Next, substrate (NPr<sub>3</sub>), H<sub>2</sub>O, and FeCl<sub>3</sub>·6H<sub>2</sub>O were sequentially added into the mixture. With each addition, the IR signal for PhCO<sub>3</sub>tBu decreased due to dilution, but remained flat, indicative of a constant concentration of the oxidant.

Finally, 2-picolinic acid (**1**) was added to the mixture, resulting in kinetic traces with increasing/decreasing slopes (green: PhCO<sub>3</sub>tBu; blue: reaction product PhCO<sub>2</sub>H; Scheme 3). Overall, these data suggest that ligand **1** is necessary for catalytic turnover and that  $\alpha$ -C-H oxidation does not occur in its absence. Importantly, the form of the kinetic traces characterizes a catalytic reaction with an initiation period. Therefore, all initial rate studies discussed below measured the maximum reaction rate (maximum slope) of the kinetic curve.

Initiation of the catalytic reaction by addition of **1** as detailed above further suggests that the empirically optimized ratio of Fe/**1** (1:1)<sup>20</sup> should also correspond to the highest observed reaction rate, if only one molecule of **1** is bound in Fe in the catalytically active species. This hypothesis was tested by measuring the initial rate with varying amounts of ligand **1** (2.5 to 10 mol %; Scheme 4). As expected, the highest initial rate was observed at a Fe/**1** ratio of 1:1, while higher and lower ratios resulted in decreased initial rates. This demonstrates that the conditions providing the highest yields are also the kinetically fastest conditions, suggesting that the active catalyst does not change throughout the course of the reaction.



**Scheme 3. In-situ FTIR Reaction Profiles of Oxidant (PhCO<sub>3</sub>tBu) and Reaction Product (PhCO<sub>2</sub>H) Demonstrating Importance of Ligand 1 for Catalysis.** Conditions: 50 °C, pyridine (50 eq.), NPr<sub>3</sub> (1 eq.), H<sub>2</sub>O (9 eq.), FeCl<sub>3</sub>·6H<sub>2</sub>O (5.0 mol %), 1 (5.0 mol %), PhCO<sub>3</sub>tBu (3 eq.).

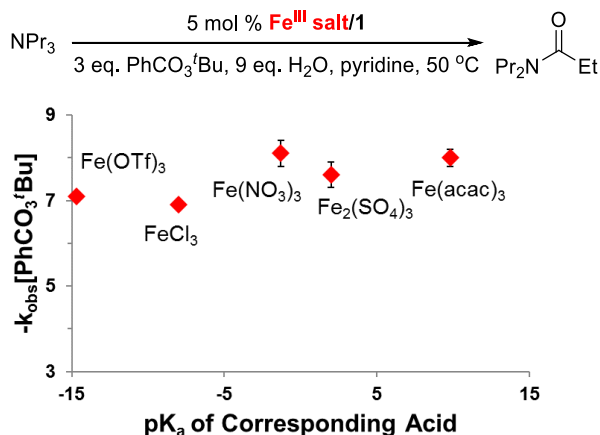


**Scheme 4. Dependence of Initial Rate on Ligand (1) Loading at Fe Loading of 5.0 mol %.**

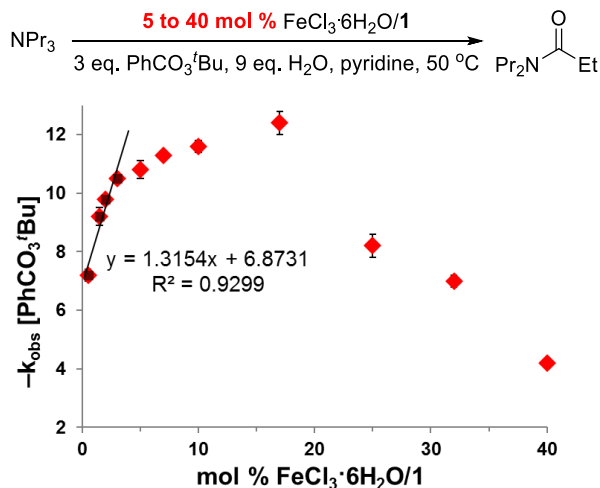
Next, we explored the influence of X-type ligands. We reasoned that the presence of these ligands can be expected to influence catalytic activity, if they remain coordinated to the Fe center. To examine this question, we measured the initial rates of the reaction with a series of Fe(III) [Fe(OTf)<sub>3</sub>, FeCl<sub>3</sub>, Fe(NO<sub>3</sub>)<sub>3</sub>, Fe<sub>2</sub>(SO<sub>4</sub>)<sub>3</sub>, Fe(acac)<sub>3</sub>] under otherwise unchanged conditions. Scheme 5 shows a plot of the resulting initial rates plotted versus the pK<sub>a</sub> of the corresponding acid of the X-type ligands. Notably, the initial rates do not change significantly, implying that X-type ligands are not coordinated to the Fe center in the catalytically active species.

We then turned our attention to establishing the kinetic orders of the different components of the catalytic system; the respective data are shown in Schemes 5 to 8. At low (catalytically relevant) concentrations of Fe/1 (<5 mol %), a nearly linear relationship was observed, suggesting that the reaction is first order in [Fe/1] under these conditions. Towards higher catalyst loadings, the measured initial rates go through a maximum. This implies that off-cycle Fe species exist that are favored under these

conditions. Such off-cycle species may be polymeric or dimeric [Fe/1]<sub>n</sub> compounds, similar to compounds that have previously been characterized in analogous Fe/1 mixtures.<sup>18</sup> Kinetic orders in [PhCO<sub>3</sub>tBu] and [NPr<sub>3</sub>] were determined in an analogous fashion. In both cases, the observed rates showed a first-order dependence, as characterized by a linear increase of rate with substrate or oxidant concentrations (see Schemes 7 and 8). At higher (not catalytically relevant) PhCO<sub>3</sub>tBu and NPr<sub>3</sub> loadings, saturation kinetics are observed (see SI).



**Scheme 5. Dependence of Initial Rate on X-Type Ligand.**

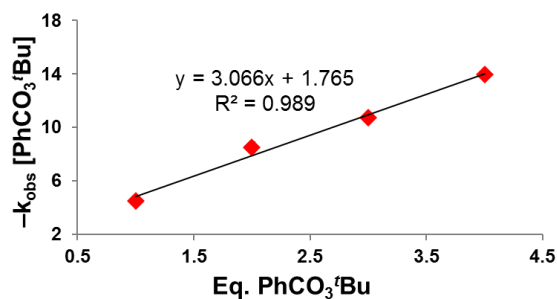
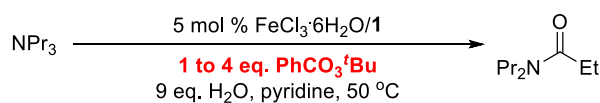


**Scheme 6. Initial Rate Versus Catalyst Loading.**

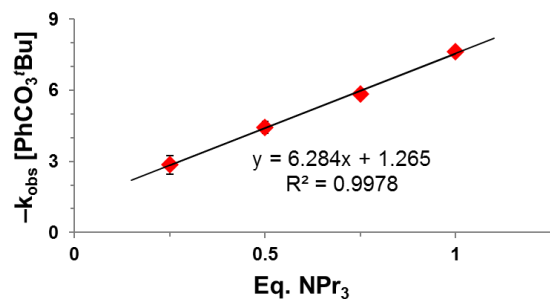
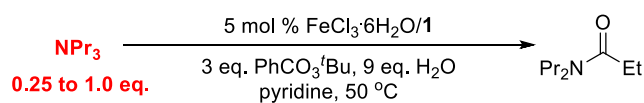
We then investigated if C-H bond cleavage may be occurring in the rds (Scheme 9) by independently measuring the initial rates of oxidation with NEt<sub>3</sub> and NEt<sub>3</sub>-D<sub>15</sub> as substrates. The obtained ratio  $k_{\text{H}}/k_{\text{D}}$  was determined to be  $1.7 \pm 0.1$ , indicative of a primary kinetic isotope effect and consistent with rate-determining C-H cleavage. Interestingly, similar values of KIEs have been observed for rate-determining  $\beta$ -hydride elimination by Ru catalysts.<sup>25</sup> Furthermore, similar ranges of isotope effects have been observed in reactions between Pd complexes and benzene/C<sub>6</sub>D<sub>6</sub>, which have been proposed to bind benzene before C-H cleavage.<sup>26</sup> Comparing these values is consistent with a mechanism in which the amine substrate binds to the Fe catalyst before C-H scission.

Next, the kinetic orders in [H<sub>2</sub>O] and [pyridine] were determined; both components of the reaction system have empirically been shown to be crucial for reactivity (Schemes 10 and

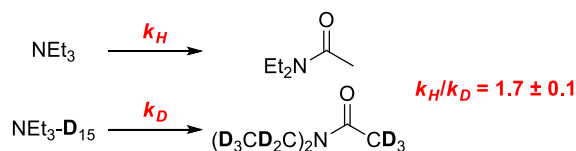
11).<sup>20</sup> Interestingly, a negative 2<sup>nd</sup> order dependence on the H<sub>2</sub>O loading is observed at low [H<sub>2</sub>O] and saturation kinetics are observed at higher [H<sub>2</sub>O]. Furthermore, a 0<sup>th</sup> order dependence on [pyridine] was observed, seemingly contradictory to the experimental observation that the absence of pyridine results in very low (EtOAc solvent) or no reactivity (all other tested solvents).



Scheme 7. Initial Rate Versus Oxidant Loading.



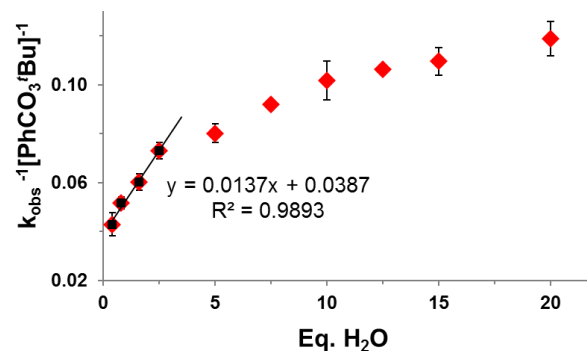
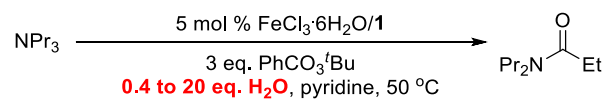
Scheme 8. Initial Rate Versus Amine Substrate Loading.



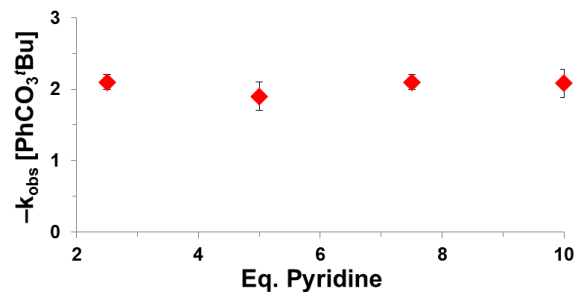
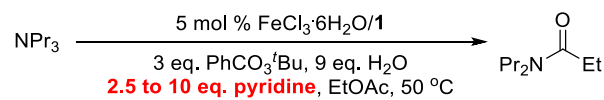
Scheme 9. Kinetic Isotope Effect Study: Initial Rate for NEt<sub>3</sub> and NEt<sub>3</sub>-D<sub>15</sub>. Conditions: 50 °C, pyridine (50 eq.), NEt<sub>3</sub> or NEt<sub>3</sub>-D<sub>15</sub> (1 eq.), H<sub>2</sub>O (9 eq.), FeCl<sub>3</sub>·6H<sub>2</sub>O (5.0 mol %), 1 (5.0 mol %), PhCO<sub>3</sub><sup>t</sup>Bu (3 eq.).

Therefore, we hypothesized that the number of coordinated pyridine ligands on Fe does not change between the resting state and the transition state structure, which is in agreement with a 0<sup>th</sup> order dependence on [pyridine]. To test this hypothesis, we performed the reaction in different substituted pyridines as solvents (50 eq. each), reasoning that coordination of pyridine-type ligands to Fe should result in a significant influence of the

ligand electronics on the catalytic rate. Such a dependence was indeed observed (Scheme 12). Interestingly, both electron-withdrawing and electron-donating substituents on pyridine result in slower initial reaction rates than pyridine, indicating a change in rds for pyridines with electron-withdrawing and electron-donating substituents.



Scheme 10. Inverse Negative Initial Rate Versus H<sub>2</sub>O Loading.

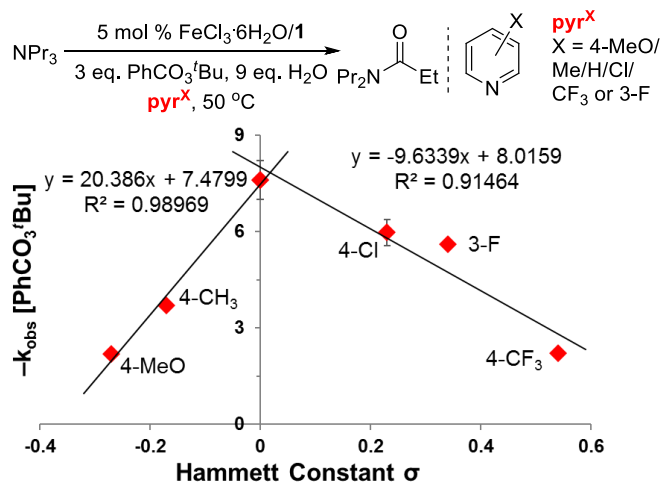


Scheme 11. Initial Rate Versus Pyridine Loading. Conditions: Conditions: 50 °C, EtOAc (50 eq.), NPr<sub>3</sub> (1 eq.), H<sub>2</sub>O (9 eq.), FeCl<sub>3</sub>·6H<sub>2</sub>O (5.0 mol %), 1 (5.0 mol %), PhCO<sub>3</sub><sup>t</sup>Bu (3 eq.), pyridine (2.5 to 10 eq.).

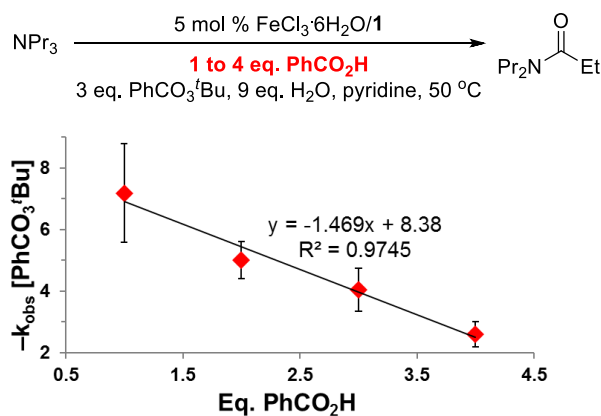
Finally, we aimed to document the kinetic orders for PhCO<sub>2</sub>H and PhCO<sub>2</sub><sup>-</sup>, as PhCO<sub>2</sub>H is a product of the reaction, which may react with the substrate in an acid-base reaction, and thus influence reaction rates. Indeed, plotting the initial rates obtained with different loadings of PhCO<sub>2</sub>H showed a negative 1<sup>st</sup> order dependence of the rate on [PhCO<sub>2</sub>H] (Scheme 13). However, all attempts to introduce PhCO<sub>2</sub><sup>-</sup> to the reaction resulted in the precipitation of alkali benzoates in solution or a rapid, non-catalyzed background reaction (NBu<sub>4</sub>PhCO<sub>2</sub>) with the oxidant. Both conditions prevent the acquisition of valid kinetic data.

**C. Further Insight into the Rate-Determining Step: Eyring Study and Oxidant Model Substrate.** To further investigate the nature of the rds, the initial rate of the reaction was measured as a function of temperature (Scheme 14) and Eyring analysis was performed to determine the activation parameters

( $\Delta H^\ddagger = 14.1$  kcal/mol;  $\Delta S^\ddagger = -10.8$  cal K<sup>-1</sup> mol<sup>-1</sup>; for details, see the SI). The obtained value for the activation entropy  $\Delta S^\ddagger$  is in agreement with a highly ordered transition state structure and is similar to values observed in concerted C-H bond cleavage processes.<sup>27,28</sup>



**Scheme 12. Hammett Studies with Different Pyridines as Solvent.**

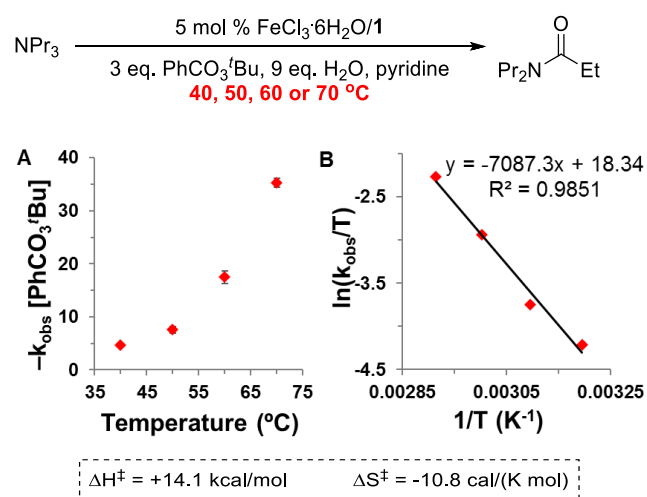


**Scheme 13. Initial Rate Versus PhCO<sub>2</sub>H Loading**

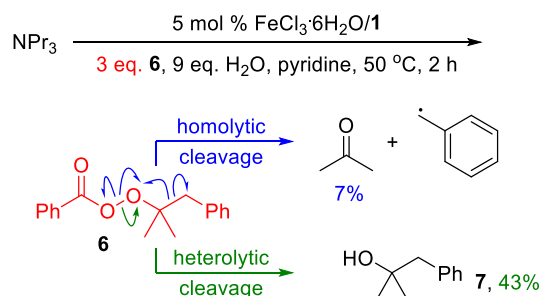
Furthermore, both activation parameters are in a similar range as activation parameters measured for rate-determining H atom transfer from substrates with weak C-H bonds to an Fe-oxo model compound ( $\Delta H^\ddagger = 12.7$  kcal/mol;  $\Delta S^\ddagger = -9$  cal K<sup>-1</sup> mol<sup>-1</sup>), albeit in combination with a significantly larger kinetic isotope effect (KIE = 5.7 for xanthene/9,10-d<sub>2</sub>-xanthene).<sup>29</sup> Generally, many metal-oxo initiated C-H bond abstractions similar to cytochrome P<sub>450</sub> (radical rebound) mechanisms show similar negative values for the activation entropy.<sup>27,30</sup> In contrast, homolytic O-O bond cleavage of peroxyesters<sup>31</sup> or reactions proceeding via dissociation of substrate from the metal catalyst prior to C-H bond cleavage<sup>32</sup> are typically associated with more positive activation entropies, corresponding to a less ordered transition state structure.

To probe the nature of oxidant participation in amine  $\alpha$ -C-H oxidation, a modified peroxyester **6** (Scheme 15) was employed as oxidant. **6** and related compounds are known to allow

differentiation between pathways that undergo homolytic and heterolytic O-O bond cleavage.<sup>33-36</sup> As outlined in Scheme 15, homolytic cleavage of the O-O bond would result in formation of acetone and a benzylic radical; interestingly, acetone was found only as a minor product (7%).



**Scheme 14. Eyring Study and Resulting Thermodynamic Activation Parameters.**



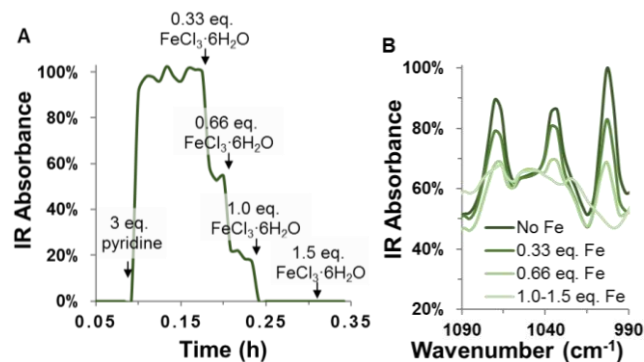
**Scheme 15. Oxidation of NPr<sub>3</sub> with Oxidant Model Substrate.** Conditions: FeCl<sub>3</sub>·6H<sub>2</sub>O (5.0 mol %), **1** (5.0 mol %), pyridine (2 mL), H<sub>2</sub>O (9.0 eq.), **6** (3.0 eq.), NPr<sub>3</sub> (1.0 eq.); yields obtained after 75% conversion of **6**. No amide product was obtained, but products of dealkylation were observed in the reaction mixture.

The major product, alcohol **7**, was obtained in 43% yield, suggesting that heterolytic O-O bond cleavage is the major reaction pathway under the established reaction conditions. This is particularly interesting, as heterolytic cleavage of the O-O bond suggests a two electron or metal-oxo pathway, which stands in contrast to free radical pathways often proposed and documented for simple Fe catalysts in the presence of other peroxy oxidants.<sup>17,37-39</sup>

**D. Coordination Studies.** To provide more insight into the resting state structure and allow future design of more reactive and selective catalyst structures, we initiated coordination studies geared towards establishing the ligand environment around the Fe catalyst precursor.

First, we sought to confirm pyridine binding (as suggested by the Hammett studies) to the Fe center. This was achieved by titrating aliquots of a solution of FeCl<sub>3</sub>·6H<sub>2</sub>O into an aqueous solution containing pyridine. The FTIR signal representing free,

non-coordinated pyridine proportionally diminished with the addition of the first two aliquots, and then disappeared with the addition of a third aliquot (Scheme 16). This result, supported by data obtained via ESI-MS analysis (see SI), indicates a pyridine: Fe binding stoichiometry of 3:1. Interestingly, the FTIR bands representing coordinated pyridine (light green spectrum labeled 1.0-1.5 eq. Fe; Scheme 16B) are very broad in comparison to the non-coordinated pyridine signals, possibly showcasing the fluxional nature of ligand coordination.

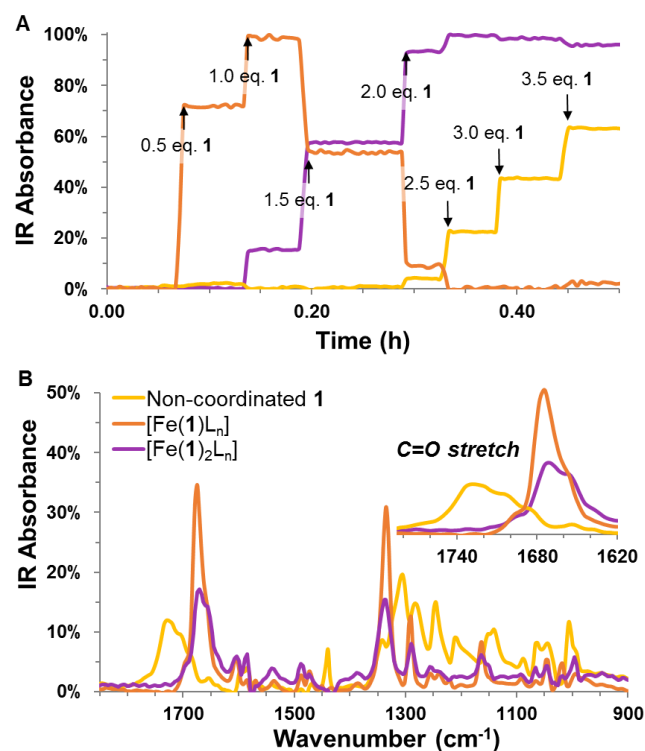


**Scheme 16. (A) *In-situ* FTIR Analysis Result of Titration of FeCl<sub>3</sub>·6H<sub>2</sub>O into Aqueous Pyridine Solution. (B) Corresponding *in-situ* FTIR Spectra.**

We next investigated binding of picolinic acid (**1**) to Fe. When aliquots corresponding to 0.5 eq. of **1** were sequentially added to a solution of 1.0 eq. FeCl<sub>3</sub>·6H<sub>2</sub>O in pyridine (Scheme 17A), *in situ* FTIR analysis showed binding with a maximum stoichiometry of 2:1 (**1**:Fe); addition of higher amounts of **1** led to the observation of a signal for non-coordinated ligand **1** (yellow trace in Scheme 17). Notably, two distinct spectra for Fe complexes of **1** were observed prior to detection of non-coordinated **1**. Both spectra are characterized by the shift of the C=O signal from 1730 cm<sup>-1</sup> (free ligand **1**) to 1690 cm<sup>-1</sup>. The first spectrum (orange trace in Scheme 17) occurs exclusively at low concentrations of **1** and constitutes the major species in solution until 1.5 eq. of **1** and disappears in the presence of 2.0 eq. of **1**. This implies that the first spectrum (orange trace) corresponds to a Fe complex [Fe(**1**)L<sub>n</sub>] with only one molecule of **1** coordinated to the metal center. The second spectrum (purple trace in Scheme 17) characterizes a complex [Fe(**1**)<sub>2</sub>L<sub>n</sub>] with two molecules of **1** as ligands. These data establish that the majority of Fe is present as [Fe(**1**)L<sub>n</sub>] at the catalytically relevant 1:1 ratio of FeCl<sub>3</sub>·6H<sub>2</sub>O and **1**.

Finally, oxidant, substrate, and product binding to [Fe(**1**)L<sub>n</sub>] were investigated. Interestingly, no significant binding to [Fe(**1**)L<sub>n</sub>] was observed for PhCO<sub>3</sub>/Bu and *N,N*-dipropyl propenamide (see SI for details). In contrast, NPr<sub>3</sub> binding to [Fe(**1**)L<sub>n</sub>] was clearly observed, as shown in Scheme 18. Upon addition of up to 1 eq. NPr<sub>3</sub> to a solution of [Fe(**1**)L<sub>n</sub>] in pyridine, a new species was detected, characterized by a C=O band at 1680 cm<sup>-1</sup> and several peaks in the fingerprint region of the FTIR spectrum (1320 to 950 cm<sup>-1</sup>, green trace in Scheme 18). This complex converts to a second species (red trace) upon addition of more NPr<sub>3</sub>; however, the first complex can still be detected until addition of 3.0 eq. of NPr<sub>3</sub> is completed. The second complex (red trace) exhibits FTIR bands in the fingerprint region that are similar to the first species but shows characteristic

new bands at 1660 and 1350 cm<sup>-1</sup> (Scheme 18B). Further addition of NPr<sub>3</sub> beyond 3.0 eq. does not result in detection of another species with distinct FTIR signals.



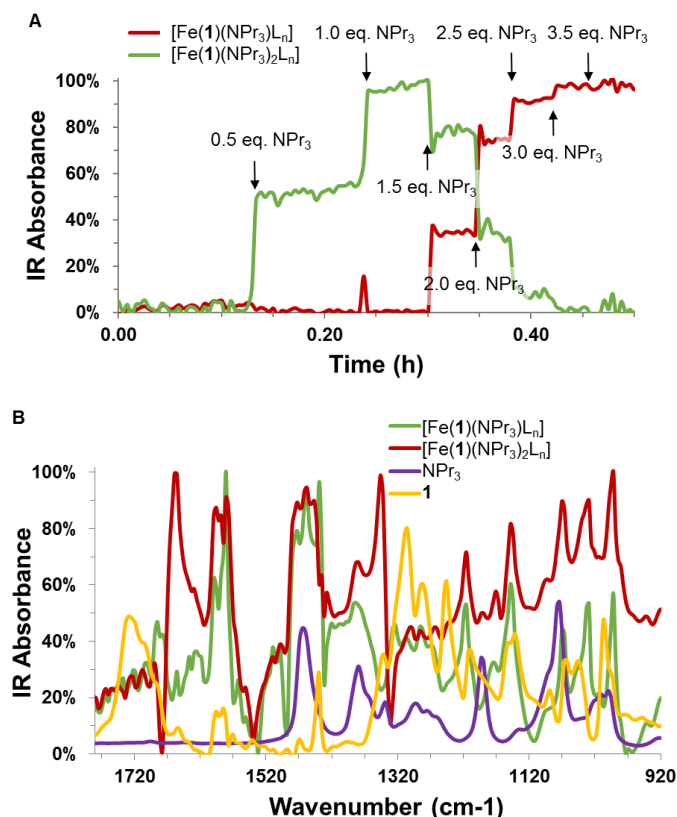
**Scheme 17. (A) Titration of **1** into FeCl<sub>3</sub>·6H<sub>2</sub>O in pyridine. (B) Comparison of observed FTIR spectra representing different [Fe(**1**)<sub>n</sub>L<sub>n</sub>] species and free picolinic acid (**1**). Color coding relates the disappearance and appearance of different spectra throughout the titration experiment.**

Due to the stoichiometry required to form each species, we propose that the first signal (green trace) corresponds to a complex [Fe(**1**)(NPr<sub>3</sub>)L<sub>n</sub>], while the second (red) trace characterizes [Fe(**1**)(NPr<sub>3</sub>)<sub>2</sub>L<sub>n</sub>] with two amine substrates as ligands. We therefore propose that up to 2 eq. of NPr<sub>3</sub> can coordinate to Fe under catalytic conditions, which are characterized by a 20-fold excess of substrate to Fe catalyst. Interestingly, the data shown in Scheme 18A imply different binding constants for the first and second equivalent of amine: The maximum amount of [Fe(**1**)(NPr<sub>3</sub>)L<sub>n</sub>] is observed with only 1 eq. of NPr<sub>3</sub> added, while addition of 2 more equivalents of NPr<sub>3</sub> is required to completely convert [Fe(**1**)(NPr<sub>3</sub>)L<sub>n</sub>] to [Fe(**1**)(NPr<sub>3</sub>)<sub>2</sub>L<sub>n</sub>].

**E. Investigation of Catalyst Initiation via Reaction Progress Kinetic Analysis.** One feature of the kinetic profiles observed in all kinetic studies discussed above is a notable initiation period. Literature precedent<sup>40</sup> suggests generally two mechanistic causes for an initiation period: (i) Promotion of catalysis by reaction products or (ii) an initial, non-catalyzed reaction, which assembles the catalytically active species.

To test if the reaction at hand is promoted by its products, a kinetic trace obtained under standard conditions (black trace in Scheme 19) was compared to kinetic traces observed upon addition of 5 mol % of different reaction products (Pr<sub>2</sub>NC(=O)Et, HNPr<sub>2</sub>, <sup>t</sup>BuOH, PhCO<sub>2</sub>H; amine dealkylation products such as HNPr<sub>2</sub> are typically observed in trace amounts in all tested

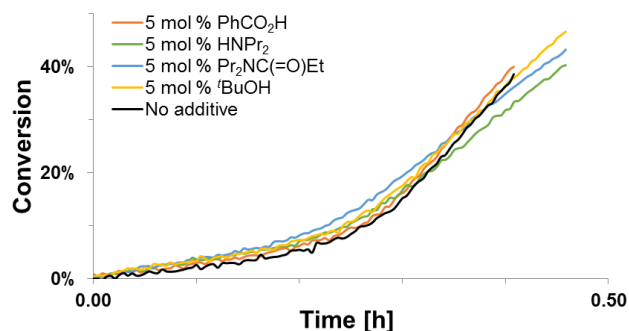
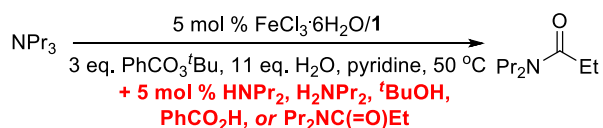
reactions<sup>20</sup>). No significant effect on either the maximum rate or the length of the initiation period was observed, as shown by the near overlap of the corresponding kinetic traces in Scheme 19. This suggests that reaction products do not promote catalysis.



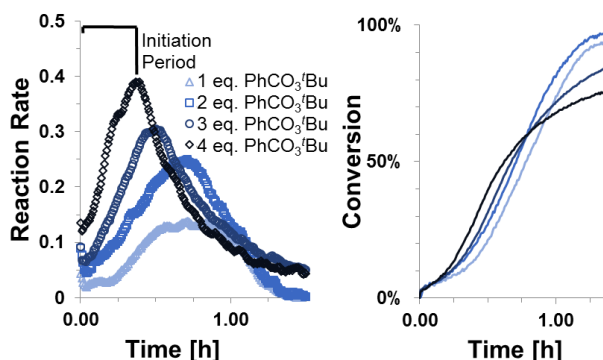
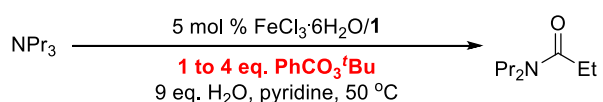
**Scheme 18.** (A) Titration of  $\text{NPr}_3$  into solution of  $[\text{Fe}(\mathbf{1})\text{L}_n]$  in pyridine. (B) Comparison of FTIR Spectra of Formed Fe Complexes, non-coordinated  $\text{NPr}_3$ , and non-coordinated  $\mathbf{1}$ .

Having ruled out the possibility of self-promotion by reaction products, we then sought to gain insight into potential off-cycle reactivity that may lead to assembly of the catalytically active species. We hypothesized that different concentrations of reagents that take part in the non-catalyzed initiation reaction should result in differing initiation period lengths. Therefore, we postulated that comparing reaction profiles obtained at different concentrations of reagents would identify reagents involved in catalyst activation. To this end, kinetic reaction profiles were plotted as reaction rate vs. time and conversion vs. time plots (Schemes 20 to 23). This analysis shows that initiation periods are shortened at *higher* [oxidant] and [substrate] and at *lower* [ $\text{H}_2\text{O}$ ] and [ $\text{PhCO}_2\text{H}$ ]. These observations suggest that these four reagents are involved in the initiation (or catalyst activation) reaction.

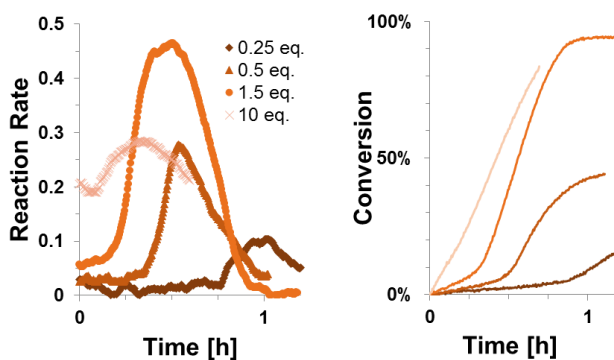
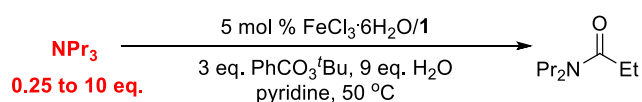
In contrast, no clear trend was observed with different loadings of  $\text{Fe}/\mathbf{1}$  (see SI), implying that the Fe catalyst concentration has no significant influence on the rate of the initiation reaction. This is in agreement with the previously stated postulate that the initiation reaction is a non-catalyzed reaction aiding in assembly of the catalytically active species.



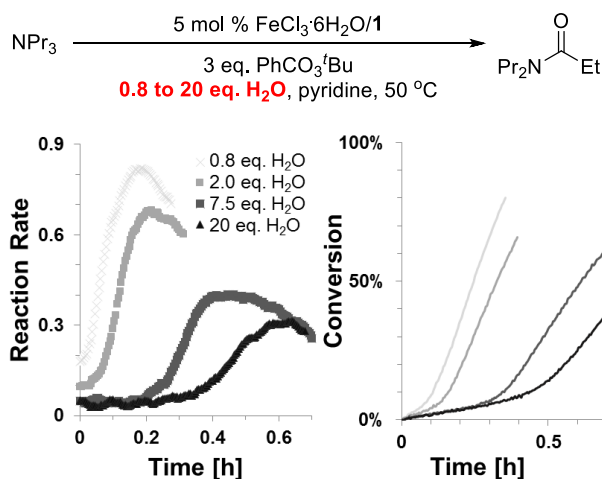
**Scheme 19.** Effect of Product Addition on Length of Initiation Period.



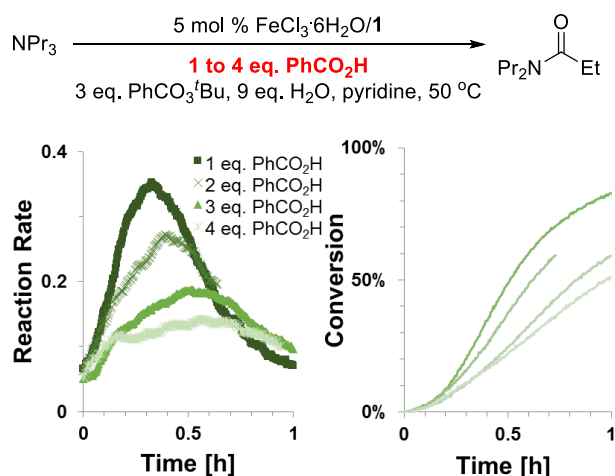
**Scheme 20.** Effect of Oxidant Loading on Length of Initiation Period.



**Scheme 21.** Effect of Amine Substrate Loading on Length of Initiation Period.



**Scheme 22. Effect of  $\text{H}_2\text{O}$  Loading on Length of Initiation Period.**



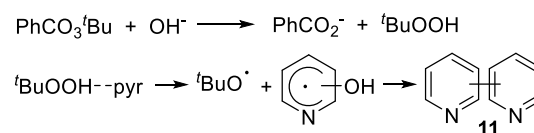
**Scheme 23. Effect of  $\text{PhCO}_2\text{H}$  Loading on Length of Initiation Period.**

Based on these data, we hypothesized that hydrolysis of the peroxyester  $\text{PhCO}_3^t\text{Bu}$  to form  $\text{PhCO}_2^-$  and  $^t\text{BuOOH}$  is the non-catalyzed reaction occurring during the initiation period (Scheme 24).  $^t\text{BuOOH}$  can go on to form  $^t\text{BuO}\cdot$  radicals in the presence of pyridine, as previously described in the literature,<sup>41-43</sup> thereby forming at least small amounts of bipyridines (**11**). This is consistent with the observation of small amounts of **11** by GCMS analysis in all amine  $\alpha\text{-C-H}$  oxidation reactions (see SI).

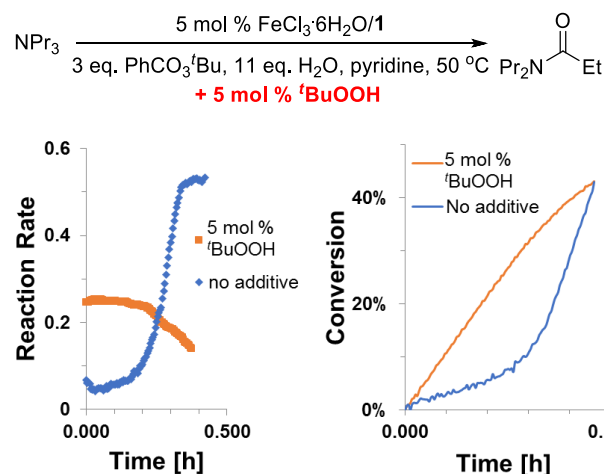
To further test the hypothesis of catalyst activation by reaction between  $^t\text{BuOOH}$  formed via hydrolysis and the Fe(III) catalyst precursor, we added 5 mol % of  $^t\text{BuOOH}$  to the reaction mixture before adding amine substrate. Gratifyingly, the kinetic trace obtained completely lacked an initiation period and the reaction initiated with a maximum rate (see Scheme 25). This suggests that formation of  $^t\text{BuOOH}$  via hydrolysis of the oxidant  $\text{PhCO}_3^t\text{Bu}$  is indeed responsible for the initiation reaction. A proposed pathway how  $^t\text{BuOOH}$  may lead to catalyst initiation is discussed *vide infra*.

**F. EPR Studies.** To gain insight into the presence of radical species and possible oxidation states of Fe in the reaction

mixture, EPR studies were performed (for complete details, see the SI). EPR studies at room temperature were designed to elucidate the proposed presence of radicals in the reaction mixture. In these studies, no radicals were observed in the absence of added  $\text{FeCl}_3$ , either via direct observation or in the presence of the spin trap phenyl-*tert*-butylnitron.



**Scheme 24. Proposed Reaction Leading to Catalyst Activation via Formation of  $^t\text{BuOOH}$  and Side Reactivity of  $^t\text{BuOOH}$ .**

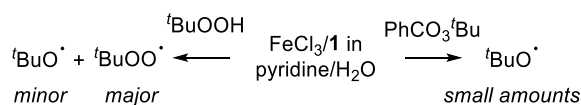


**Scheme 25. Effect of  $^t\text{BuOOH}$  Addition on Length of Initiation Period.**

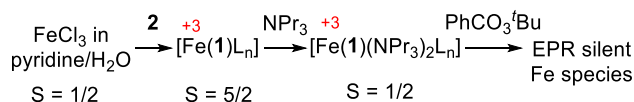
In a mixture of  $\text{FeCl}_3$ , **1**, pyridine, and water (mimicking the catalytic reaction mixture), addition of either  $^t\text{BuOOH}$  or  $\text{PhCO}_3^t\text{Bu}$  resulted in formation of O-centered radicals, but in different amounts and selectivity (Scheme 26A). With  $^t\text{BuOOH}$ , the major radical detected was  $^t\text{BuOO}\cdot$ , while only small amounts of  $^t\text{BuO}\cdot$  were detected upon addition of  $\text{PhCO}_3^t\text{Bu}$ . This suggests that  $^t\text{BuOO}\cdot$  may be the product of the catalyst activation pathway. Furthermore, the data imply that small amounts of  $\text{PhCO}_3^t\text{Bu}$  can undergo homolytic O-O bond scission in the presence of Fe(III), even though the majority of turnover in C-H oxidation stems from heterolytic O-O bond cleavage, as evidenced by the oxidant model study described further above.

EPR studies to elucidate the spin state of the Fe center were performed on solutions frozen in liquid nitrogen immediately after preparation. EPR clearly shows the binding of ligand **1** upon addition of **1** to a  $\text{FeCl}_3$  solution in pyridine/ $\text{H}_2\text{O}$ , with a new high-spin signal ( $S = 5/2$ ). Addition of  $\text{NPr}_3$  to this solution resulted in a low-spin Fe species ( $S = 1/2$ ) with a very broad signal at  $g = 2$ . Both of these findings are in agreement with ligand binding to Fe(III) as proposed by FTIR titration (see above). Interestingly, when  $\text{PhCO}_3^t\text{Bu}$  is added to the resulting mixture, no EPR signal is observed, suggesting the formation of an EPR silent species as the resting state of the reaction.

### A. Radicals as detected by EPR at room temperature



### B. Fe spin states as detected by EPR at 135 K.



Scheme 26. Summary of Results from EPR Studies.

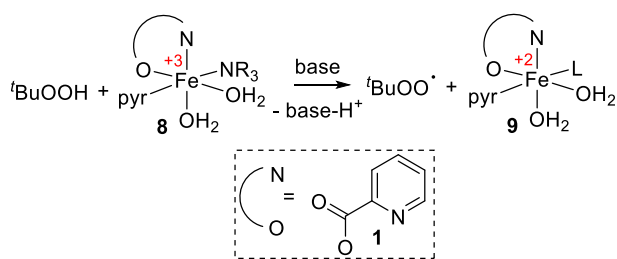
**G. Discussion of Mechanistic Proposals Based on Experimental Data.** Based on the experimental mechanistic data obtained, we propose (i) a mechanistic pathway for catalyst activation and (ii) two catalytic cycles for catalyst turnover.

First, catalyst activation is clearly achieved by the interaction of the Fe(III) catalyst precursor **8** and <sup>t</sup>BuOOH. As evidenced by EPR studies, the formation of <sup>t</sup>BuOO• likely occurs in this reaction, suggesting a reduction from Fe(III) to Fe(II) in a reaction step preceded in Fenton chemistry.<sup>22</sup> In combination with the ligand coordination studies, this leads to a proposed resting state structure **9** as shown in Scheme 27.

Based on this resting state structure, two different catalytic cycles (Scheme 28A/B) can be proposed that fulfill the empirical rate law (Scheme 28C), the requirement for heterolytic O-O bond cleavage, <sup>18</sup>O labeling being introduced to the product from <sup>18</sup>O-labeled water,<sup>20</sup> and C-H bond scission in the rds. Both catalytic cycles (A and B) start with similar resting states **9** and **9a**, with the only difference being one molecule of water being associated with the resting state in mechanism B. Due to the catalytic relevance of ligand **1**, we propose that it remains coordinated to Fe throughout the complete catalytic cycle. Coordination of pyridine, two H<sub>2</sub>O ligands, and one molecule of a spectator ligand complete the resting state structures. Due to the significantly lower reaction rates at high [Fe/1], we propose that each resting state is in equilibrium with an off-cycle, oligomeric or polymeric species [Fe(I)L<sub>x</sub>]<sub>n</sub>. The key difference between mechanisms A and B lies in (i) the Fe species affecting the C-H scission and (ii) oxidation state changes throughout the catalytic cycle.

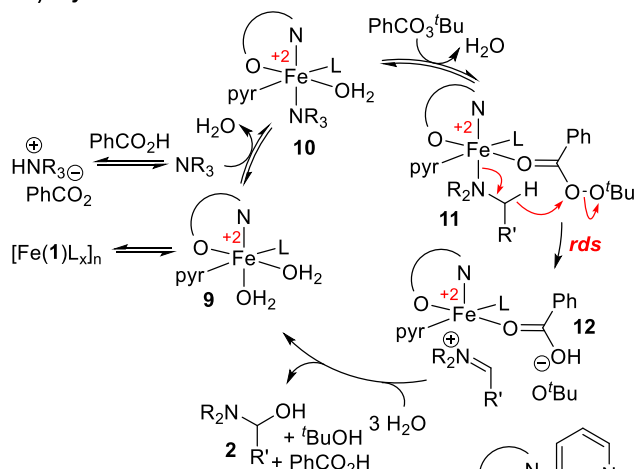
Mechanism A is characterized by a series of coordination/dissociation steps between resting state **9** and rds, with the rds proceeding through a hybrid between β-hydride elimination and concerted metalation/deprotonation. The oxidant O-O bond is cleaved in the rds concurrently with the C-H bond, while the oxidant also acts as an internal base to aid in β-hydride elimination of the amine, resulting in an iminium salt as product. During the complete cycle A, Fe remains in the oxidation state +2.

Mechanism B also proceeds through a series of coordination/dissociation steps between the resting state **9a** and the rds, in addition to a two electron-oxidation of Fe(+2) to Fe(+4). This oxidation proceeds upon heterolytic O-O bond cleavage of PhCO<sub>3</sub><sup>t</sup>Bu, in agreement with the model oxidant studies discussed above. The rds in mechanism B is formulated analogous to typical radical-rebound mechanisms at Fe-oxo species, consisting of a homolytic C-H bond cleavage at Fe(+4) intermediate **13**, followed by a fast rebound step to directly produce the bound hemiaminal intermediate.

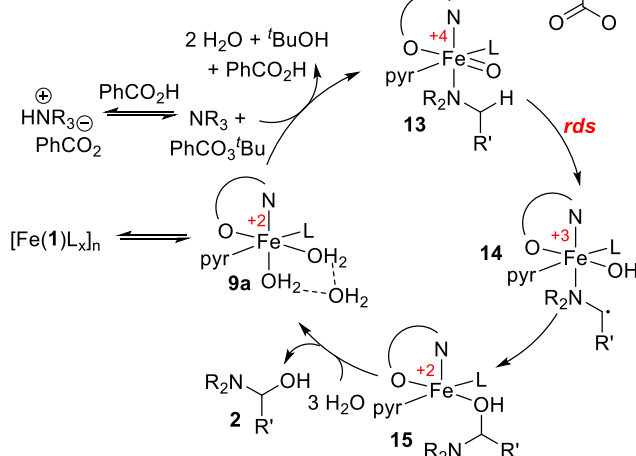


Scheme 27. Catalyst Activation and Proposed Resting State Structure **9**.

### A. β-Hydride Elimination/CMD Mechanism.



### B. Fe-Oxo Mechanism.



### C. Empirical Rate Law

$$\text{rate} \sim [\text{NPr}_3][\text{PhCO}_3{}^t\text{Bu}][\text{Fe}/1][\text{H}_2\text{O}]^{-2}[\text{PhCO}_2\text{H}]^{-1}[\text{pyridine}]^0$$

Scheme 28. Proposed Catalytic Cycles Based on Experimental Mechanistic Studies.

### Summary and Conclusions

Overall, the results of the mechanistic studies can be graphically summarized in detailed proposed mechanisms as shown in Scheme 28. Several general conclusions can be drawn from the two proposed mechanisms: (1) Both pyridine and ligand **1** do not dissociate from the catalytically active species throughout both cycles. This suggests a path forward in the journey

towards more efficient catalysts (and away from pyridine in solvent-quantities): The design of a ligand in which **1** is covalently associated with a pyridine moiety. (2) Kinetic profiling and EPR studies allowed the proposal of **9** as the reagent providing access to the catalytically active species **9**. This suggests that one-electron reduction is required to access the catalytically active species, which in turn might simply be achieved by the use of Fe(+2) catalyst precursor species. (3) The two presented mechanisms consistent with the experimental data do not suggest a role for free radicals in the reaction mechanism outside of the catalyst activation pathway. This fundamentally distinguishes the investigated catalyst system from the systems investigated previously by Doyle and coworkers.<sup>19</sup> The presented work further provides an explanation for why  $\alpha$ -C-H oxidation of a wide variety of tertiary aliphatic amines is possible: coordination to Fe activated the substrate to undergo C-H cleavage. In contrast, previous systems proceeding through free radical mechanisms are restricted to more activated substrates (secondary amines, benzylic/aniline-type substrates). (4) Remaining questions regarding the mechanism (e.g. distinguishing between the two proposed mechanisms; the specifics of oxidant/Fe interactions; or the source of the catalyst system's unique selectivity for acyclic amines) will likely require further in-depth spectroscopic and DFT studies.

## ASSOCIATED CONTENT

**Supporting Information.** Detailed procedures for kinetic and coordination studies, examples of kinetic traces, ESI-MS and GCMS analyses. This material is available free of charge via the Internet at <http://pubs.acs.org>.

## AUTHOR INFORMATION

### Corresponding Author

\* mhemmert@wpi.edu; marion.emmert@merck.com

### Author Contributions

The manuscript was written through contributions of all authors. All authors have given approval to the final version of the manuscript.

## ACKNOWLEDGMENT

We thankfully acknowledge R. Grimm (WPI) for assistance with ESI-MS measurements, D. Hebrault and M. Burns (both Mettler-Toledo) for assistance with acquiring *in-situ* FTIR analyses, and M. Frenette (UQAM) for helpful discussions. We acknowledge Worcester Polytechnic Institute for financial support of this work.

## REFERENCES

- (1) Chen, K.; Baran, P. S., *Nature* **2009**, *459*, 824-828.
- (2) Genovino, J.; Sames, D.; Hamann, L. G.; Touré, B. B., *Angew. Chem. Int. Ed.* **2016**, *55*, 14218-14238.
- (3) Oscarson, M., *Drug Metab. Dispos.* **2001**, *29*, 91-95.
- (4) Walsh, A. A.; Szklarz, G. D.; Scott, E. E., *J. Biol. Chem.* **2013**, *288*, 12932-12943.
- (5) Nam, W., *Acc. Chem. Res.* **2007**, *40*, 522-531.
- (6) Schlichting, I.; Berendzen, J.; Chu, K.; Stock, A. M.; Maves, S. A.; Benson, D. E.; Sweet, R. M.; Ringe, D.; Petsko, G. A.; Sligar, S. G., *Science* **2000**, *287*, 1615-1622.
- (7) Chen, K.; Que, L., *J. Am. Chem. Soc.* **2001**, *123*, 6327-6337.
- (8) Groves, J. T., *Nature Chem.* **2014**, *6*, 89-91.
- (9) Huang, X.; Groves, J. T., *J. Biol. Inorg. Chem.* **2017**, *22*, 185-207.
- (10) Chiavarino, B.; Cipollini, R.; Crestoni, M. E.; Fornarini, S.; Lanucara, F.; Lapi, A., *J. Am. Chem. Soc.* **2008**, *130*, 3208-3217.
- (11) Li, Z.; Bohle, D. S.; Li, C.-J., *Proc. Natl. Acad. Sci.* **2006**, *103*, 8928-8933.
- (12) Catino, A. J.; Nichols, J. M.; Nettles, B. J.; Doyle, M. P., *J. Am. Chem. Soc.* **2006**, *128*, 5648-5649.
- (13) Boess, E.; Schmitz, C.; Klusmann, M., *J. Am. Chem. Soc.* **2012**, *134*, 5317-5325.
- (14) Boivin, J.; Gaudin, D.; Labrecque, D.; Jankowski, K., *Tetrahedron Lett.* **1990**, *31*, 2281-2282.
- (15) Barton, D. H. R.; Boivin, J.; Gaudin, D.; Jankowski, K., *Tetrahedron Lett.* **1989**, *30*, 1381-1382.
- (16) Barton, D. H. R.; Doller, D., *Acc. Chem. Res.* **1992**, *25*, 504-512.
- (17) Perkins, M. J., *Chem. Soc. Rev.* **1996**, *25* (4), 229-236.
- (18) Kiani, S.; Tapper, A.; Staples, R. J.; Stavropoulos, P., *J. Am. Chem. Soc.* **2000**, *122*, 7503-7517.
- (19) Ratnikov, M. O.; Doyle, M. P., *J. Am. Chem. Soc.* **2013**, *135*, 1549-1557.
- (20) Legacy, C. J.; Wang, A.; O'Day, B. J.; Emmert, M. H., *Angew. Chem. Int. Ed.* **2015**, *54*, 14907-14910.
- (21) Yilmaz, O.; Oderinde, M. S.; Emmert, M. H., *J. Org. Chem.* **2018**, *83*, 11089-11100.
- (22) (a) Sawyer, D. T.; Sobkowiak, A.; Matsushita, T., *Acc. Chem. Res.* **1996**, *29*, 409-416; (b) MacFaul, P. A.; Wayner, D. D. M.; Ingold, K. U., *Acc. Chem. Res.* **1998**, *31*, 159-162; Goldstein, S.; Meyerstein, D., *Acc. Chem. Res.* **1999**, *32*, 547-550.
- (23) Davies, D. L.; Donald, S. M.; Macgregor, S. A., *J. Am. Chem. Soc.* **2005**, *127*, 13754-13755.
- (24) Boutadla, Y.; Davies, D. L.; Macgregor, S. A.; Poblador-Bahamonde, A. I., *Dalton Trans.* **2009**, 5820-5831.
- (25) Thalen, L. K.; Zhao, D.; Sortais, J. B.; Paetzold, J.; Hoben, C.; Backvall, J. E., *Chem. Eur. J.* **2009**, *15*, 3403-3410.
- (26) Zhong, H. A.; Labinger, J. A.; Bercaw, J. E., *J. Am. Chem. Soc.* **2002**, *124*, 1378-1399.
- (27) Gardner, K.; Mayer, J., *Science* **1995**, *269*, 1849-1851.
- (28) Roiban, G. D.; Serrano, E.; Soler, T.; Aullon, G.; Grosu, I.; Cativiela, C.; Martinez, M.; Urriolabeitia, E. P., *Inorg. Chem.* **2011**, *50*, 8132-8143.
- (29) Cho, K.; Leeladee, P.; McGown, A. J.; DeBeer, S.; Goldberg, D. P., *J. Am. Chem. Soc.* **2012**, *134*, 7392-7399.
- (30) Cook, G. K.; Mayer, J. M., *J. Am. Chem. Soc.* **1995**, *117*, 7139-7156.
- (31) Kim, S. S.; Baek, I. S.; Tuchkin, A.; Go, K. M., *J. Org. Chem.* **2001**, *66*, 4006-4011.
- (32) Jones, W. D.; Feher, F. J., *Acc. Chem. Res.* **2002**, *22*, 91-100.
- (33) Hedaya, E.; Winstein, S., *J. Am. Chem. Soc.* **1967**, *89*, 1661-1672.
- (34) Foster, T. L.; Caradonna, J. P., *J. Am. Chem. Soc.* **2003**, *125*, 3678-3679.
- (35) Rowe, G. T.; Rybak-Akimova, E. V.; Caradonna, J. P., *Chem. Eur. J.* **2008**, *14*, 8303-8311.
- (36) Makhlynets, O. V.; Rybak-Akimova, E. V., *Chem. Eur. J.* **2010**, *16*, 13995-14006.
- (37) Sawyer, D. T.; Sobkowiak, A.; Matsushita, T., *Acc. Chem. Res.* **1996**, *29*, 409-416.
- (38) MacFaul, P. A.; Wayner, D. D. M.; Ingold, K. U., *Acc. Chem. Res.* **1998**, *31*, 159-162.
- (39) Goldstein, S.; Meyerstein, D., *Acc. Chem. Res.* **1999**, *32*, 547-550.
- (40) Blackmond, D. G., *J. Am. Chem. Soc.* **2015**, *137*, 10852-10866.
- (41) Zolotova, N. V.; Denisov, E. T., *Bull. Acad. Sci. USSR, Div. Chem. Sci.* **1966**, *15*, 736-738.
- (42) Steenken, S.; O'Neill, P., *J. Phys. Chem.* **1978**, *82* (3), 372-374.
- (43) Maillard-Dupuy, C.; Guillard, C.; Courbon, H.; Pichat, P., *Environ. Sci. Technol.* **1994**, *28*, 2176-2183.